

RESEARCH ARTICLE

Impacts of Typhoon Megi (2010) on the South China Sea

10.1002/2013JC009785

Dong Shan Ko¹, Shenn-Yu Chao², Chun-Chieh Wu³, and I-I Lin³

Special Section:

Pacific-Asian Marginal Seas

¹Oceanography Division, Naval Research Laboratory, Stennis Space Center, Mississippi, USA, ²Horn Point Laboratory, University of Maryland Center for Environmental Science, Cambridge, Maryland, USA, ³Department of Atmospheric Sciences, National Taiwan University, Taipei, Taiwan

Key Points:

- Cold wake induced by typhoon Megi
- Monsoon and beta effect contributed to the westward shift of cold wake

Correspondence to:

D. S. Ko,
dong.ko@nrlssc.navy.mil

Citation:

Ko, D. S., S.-Y. Chao, C.-C. Wu, and I-I Lin (2014), Impacts of Typhoon Megi (2010) on the South China Sea, *J. Geophys. Res. Oceans*, 119, doi:10.1002/2013JC009785.

Received 30 DEC 2013

Accepted 19 JUN 2014

Accepted article online 23 JUN 2014

Abstract In October 2010, typhoon Megi induced a profound cold wake of size 800 km by 500 km with sea surface temperature cooling of 8°C in the South China Sea (SCS). More interestingly, the cold wake shifted from the often rightward bias to both sides of the typhoon track and moved to left in a few days. Using satellite data, in situ measurements and numerical modeling based on the East Asian Seas Nowcast/Forecast System (EASNFS), we performed detailed investigations. To obtain realistic typhoon-strength atmospheric forcing, the EASNFS applied typhoon-resolving Weather Research and Forecasting (WRF) model wind field blended with global weather forecast winds from the U.S. Navy Operational Global Atmospheric Prediction System (NOGAPS). In addition to the already known impacts from the slow typhoon translation speed and shallow pre-existing ocean thermocline, we found the importance of the unique geographical setting of the SCS and the NE monsoon. As the event happened in late October, NE monsoon already started and contributed to the southwestward ambient surface current. Together with the topographic β effect, the cold wake shifted westward to the left of Megi's track. It was also found that Megi expelled waters away from the SCS and manifested as a gush of internal Kelvin wave exporting waters through the Luzon Strait. The consequential sea level depression lasted and presented a favorable condition for cold dome development. Fission of the north-south elongated cold dome resulted afterward and produced two cold eddies that dissipated slowly thereafter.

1. Introduction

Typhoon Megi (2010) was one of the most intense tropical cyclones on record and the only category-5 typhoon in the Saffir-Simpson scale in 2010. It became typhoon around midday 14 October at western North Pacific, at 0000 UTC 17 October, Megi intensified to the highest intensity category of 5 or Super Typhoon (Figure 1). At its peak, Megi's 1 min maximum sustained wind speed reached 160 kt (82.5 m/s) and sea level air pressure at center dropped to 903 hPa according to Joint Typhoon Warning Center (JTWC; <http://www.usno.navy.mil/JTWC/>). Early on 18 October, Megi made its first landfall over Luzon, Philippines. By passing Luzon, Megi entered the South China Sea (SCS) around 1500 UTC 18 October. It weakened to category-3 over land but regained back to the category-4 intensity after entering the SCS. An intense cold wake with enhanced biological activities was induced and left behind its trail [Chen *et al.*, 2012]. Megi made its second landfall over southeast China at about 0600 UTC 23 October and gradually dissipated afterward. Under the sponsorship of U.S. Office of Naval Research and Taiwan's National Science Council, Megi was well observed by airborne and seagoing measurements as a part of the ITOP international project [D'Asaro *et al.*, 2011, 2013; Pun *et al.*, 2011]. The acronym stood for "Impact of Typhoons on the Ocean in the Pacific" in the United States and "Internal wave and Typhoon-Ocean interaction Project in the Western North Pacific and Neighboring Seas" in Taiwan.

Typhoon impact on the SCS has drawn much interest for more than a decade [Chu *et al.*, 2000; Lin *et al.*, 2003a, 2003b; Zheng and Tang, 2007; Shang *et al.*, 2008; Tseng *et al.*, 2010; Chiang *et al.*, 2011; Chen *et al.*, 2012]. For example, the intense cold wake (9–11°C cooling) of typhoon Kai-Tak (2000) and Lingling (2001) was found to be associated with strong upwelling due to slow typhoon translation speed and to shallow pre-existing ocean thermocline [Lin *et al.*, 2003a; Shang *et al.*, 2008; Tseng *et al.*, 2010; Chiang *et al.*, 2011]. Some of the past numerical studies [e.g., Chu *et al.*, 2000; Tseng *et al.*, 2010; Chiang *et al.*, 2011] employed global forecasted winds, satellite-derived winds, or a mixture of both to assess the typhoon-induced impact. As typhoon structure and intensity may not be adequately resolved in the global-scale wind products, we employ in this research typhoon-scale resolving wind.

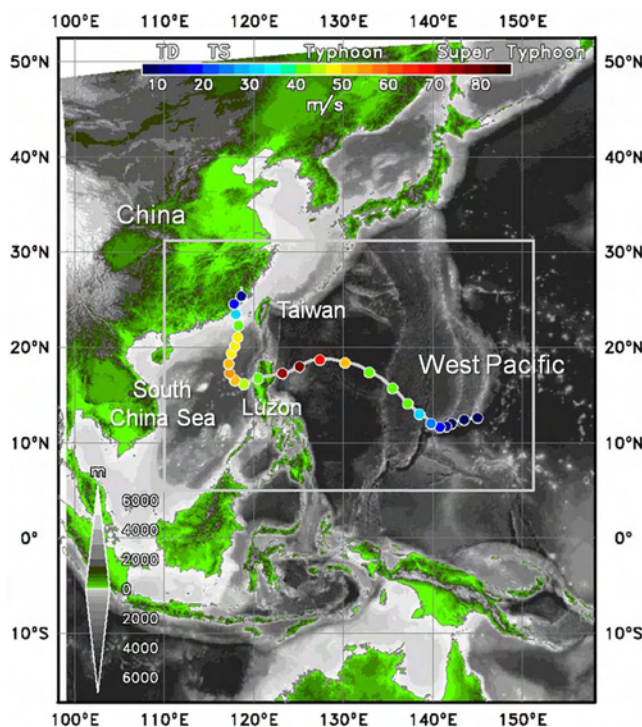


Figure 1. The EASNFS model domain with topography and an inset covered by WRF model. Typhoon Megi's track (from JTWC best-track) is dotted semidaily at 0000 and 1200 UTC with color indicating maximum sustained wind speed.

In addition, the SCS is an almost enclosed basin with narrow straits connecting to both Pacific and Indian Oceans. The confinement arises from land masses and straits, most of latter are shallow except the Luzon Strait. With this unique geographical setting, we also intend to explore the contribution of this partial confinement.

The ocean precondition at 0000 UTC 15 October, when Megi was still far east of the SCS over the western North Pacific Ocean, is illustrated in Figure 2. The Multi-Channel Sea Surface Temperature (MCSST) shows warmer sea surface temperature (SST) in the western North Pacific Ocean and SCS south of China coast (Figure 2a). The cool water invaded China coastal water from north due to onset of winter monsoon at this time.

The composite altimeter Sea Surface Height (SSH) shows lower sea level over the northern SCS and China coastal water (Figure 2b). The temperature section at 18°N derived from the East Asian Seas Nowcast/Forecast System, partially separated by a north-south line of volcanoes across the Luzon Strait, indicates a much shallower SCS thermocline on the west side relative to the western North Pacific thermocline on the east side (Figure 2c).

Figure 3, derived from the cloud-penetrating SST observations from the Advanced Microwave Sounding Radiometer for the Earth Observing System (AMSR-E) and the Tropical Rainfall Measuring Mission (TRMM) Microwave Imager (TMI) [Wentz *et al.*, 2000], shows selected daily mean SST before, during, and after Megi's passage over SCS. The U.S. Joint Typhoon Warning Center's (JTWC) best-track typhoon data of Megi are color-coded by dots to indicate Megi's intensity at every 6 h. After entering the SCS, Megi followed an essentially northward track and left a trail of north-south elongated intense cold wake behind. As indicated in the SST time series at a fixed location off northwest Luzon (Figure 3, bottom), cooling ranged up to 8°C. The cold anomaly persisted long after Megi made its landfall on southeast China. A post-Megi XBT in situ survey was conducted by Taiwan's research vessel, Ocean Research 1 (OR1), on 25 October. The XBT observation revealed concurrent isotherm doming underneath the cold anomaly and will be shown and discussed later in section 7, in the context of cold dome fission (Figure 14).

Figure 4, based on Archiving, Validation, and Interpretation of Satellite Oceanographic data (AVISO), shows difference in the sea surface height anomalies (SSHA) induced by Megi. Through subtracting weekly mean SSHA pre-Megi (from 6 October to 12 October) and post-Megi's passing of the SCS, Figure 4 was obtained.

Notable developments are two large sea surface depressions or cold wakes: a strong one in the SCS and a much weaker one east of Luzon at the Philippine Sea. The time averaging after Megi's entrance to the SCS (from 20 October to 26 October) might have slightly favored the appearance of the cold wake in the SCS with reduced time lag relative to the corresponding cold wake on the Pacific side. However, it should not be the primary cause of the lopsided distribution. As confirmed by Lin *et al.* [2013], the much deeper thermocline over the Philippine Sea as well as Megi's much faster translation speed (typically ~7 m/s) caused minimal ocean response. The SST cooling was only ~1°C. Sequential SST snapshots, of which only a

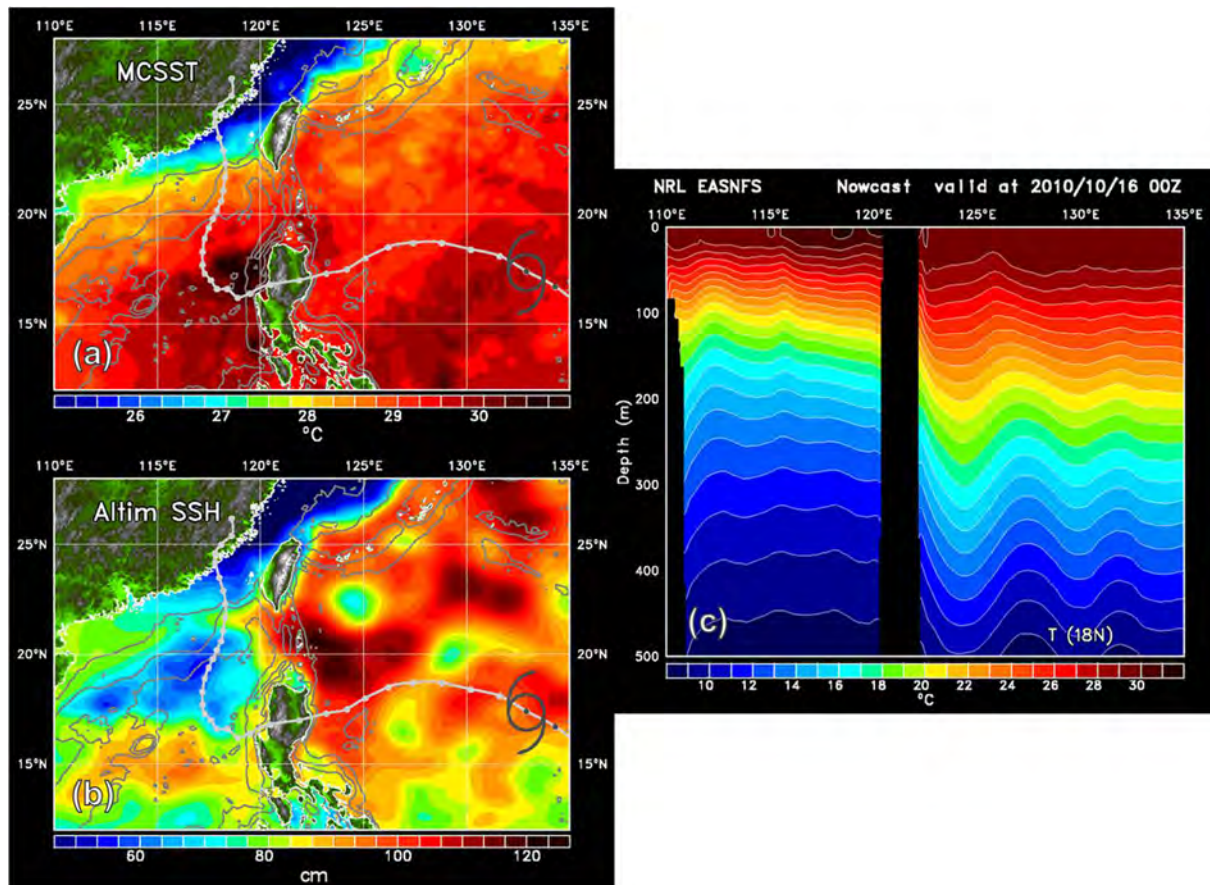


Figure 2. Ocean precondition at 0000 UTC 15 October 2010 and 6 h dotted Megi's track: (a) MCSST, (b) altimeter SSH, and (c) EASNFS temperature section at 18°N. Hurricane symbol in Figures 2a and 2b marks the contemporaneous eye location. Also shown in Figures 2a and 2b are 100, 1000, and 3000 m isobaths. Though SST at SCS was higher than western North Pacific Ocean, the thermocline was much shallower indicated by lower altimeter SSH and temperature cross section from EASNFS.

selected few are shown in Figure 3, consistently shows stronger and long-lasting appearance of Megi's cold wake in the SCS.

Megi was more intense over the Pacific Ocean than over the SCS (Figure 4). The weakened typhoon over the SCS does not seem able to fully account for the disproportionate intense cold wake. Rather, satellite observations and ocean modeling (to be discussed below) indicated much reinvigorated cold wake strength and tenacity in the SCS. This somewhat counterintuitive response motivated the present study. We did so by simulating ocean responses to a high-resolution wind forcing that adequately resolved Megi's intensity.

The paper is organized as follows. The ocean model is described in section 2. The Megi-resolving atmospheric forcing is described in section 3. The SCS response to Megi is discussed in section 4. The internal Kelvin wave around Luzon and its role in expelling waters from the SCS and cold wake enhancement are discussed in section 5. The relationship between cold dome development and Luzon Strait transport variation is examined in section 6. Discussion of cold dome fission and its westward movement after Megi's landfall is given in section 7. Section 8 concludes this work.

2. Ocean Model

The East Asian Seas Nowcast/Forecast System (EASNFS) was used for this study. EASNFS is an application of the U.S. NRL's Ocean Nowcast/Forecast System [Ko *et al.*, 2008]. The dynamic ocean model in the EASNFS is the U.S. Navy Coastal Ocean Model (NCOM) [Martin, 2000], developed at Naval Research Laboratory and

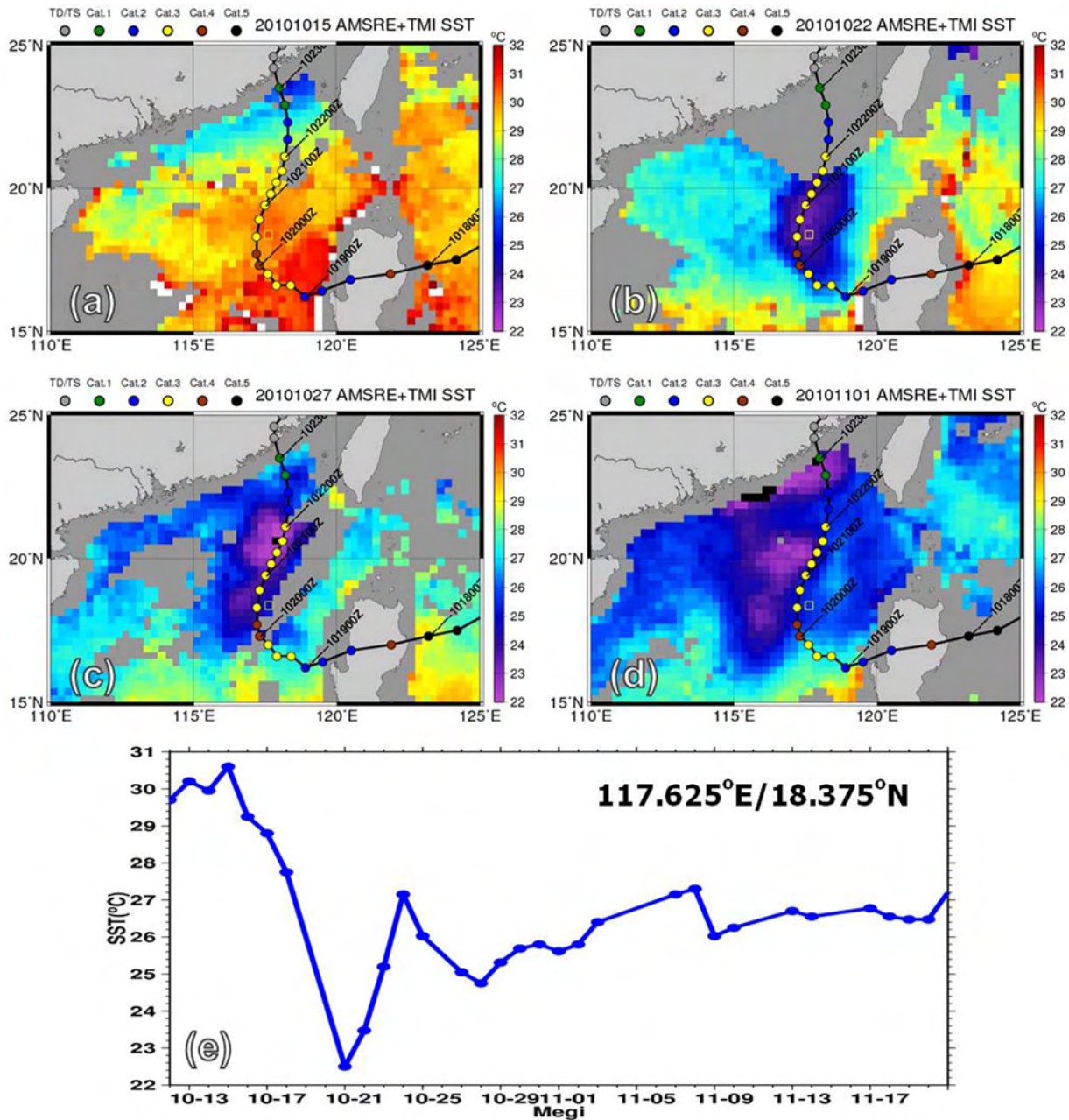


Figure 3. Selected daily mean SST at SCS, derived from AMSRE and TMI, and the JWC best-track of Megi with color coded dots indicating the strength. The bottom plot shows SST variation at 117.625°E, 18.375°N (denoted in top four plots as the yellow square to the right of Megi's track) during and after Megi's passage. Strong surface cooling was during the onset of Megi. Cold wake spreaded on both side of track. It moved westward and broke up into two cold eddies afterward.

in operation at Naval Oceanography Office. A statistical regression model, the Modular Ocean Data Assimilation System (MODAS) [Carnes et al., 1996; Fox et al., 2002] based on historical observations, is used to produce the three-dimensional ocean temperature and salinity analyses from satellite altimetry and multichannel sea surface temperature observations. EANSFS then assimilates the analyses by continuous modification of model temperature and salinity toward the analyses using a vertical weighting function that reflects the oceanic temporal and spatial correlation scales and the relative confidence between the model forecasts and analyses. In addition, scale separation is applied in data assimilation to preserve the fast-varying components.

The EANSFS model domain covers the entire East Asian marginal seas and part of the Western Pacific Ocean with domain from 17.3°S to 52.2°N and from 99.2°E to 158.2°E (Figure 1). The horizontal resolution is ~1/12°

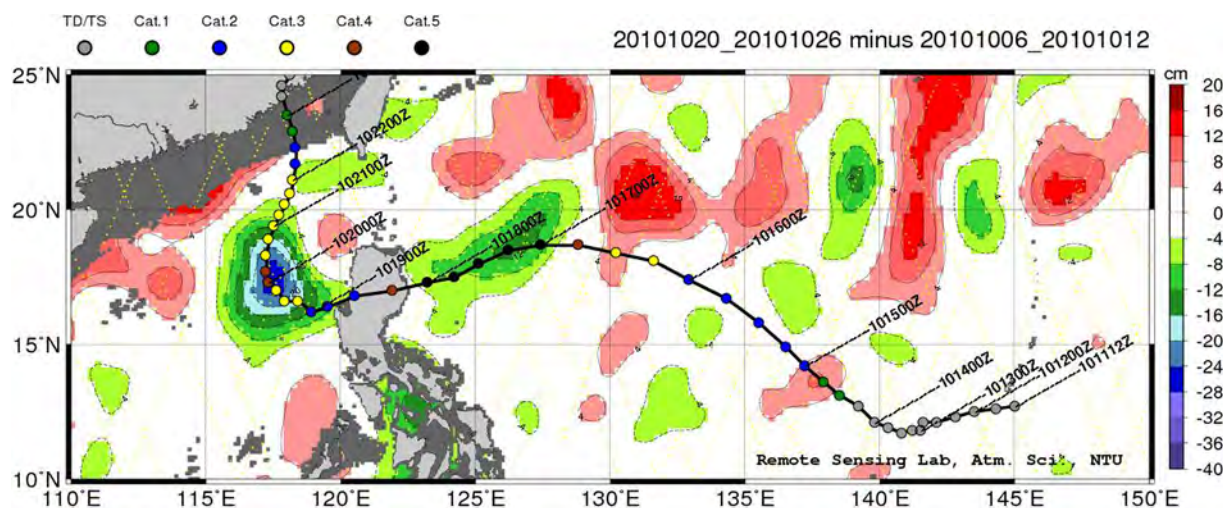


Figure 4. JTWC best-track of Megi with color-coded dots indicating its strength. Color-shaded contours at intervals of 5 cm indicate time-averaged sea surface height anomalies (SSHA) near Megi. The anomalies are derived by subtracting pre-Megi mean SSHA (from 6 October to 12 October) from mean SSHA (from 20 October to 26 October) after Megi entered the South China Sea.

that ranges from ~ 9.8 km at the equator to ~ 6.5 km at the model's northern boundary. The horizontal resolution is about 9 km in the study region. There are 41 sigma- z levels with denser levels in the upper water column to gain resolution. EASNFS analysis has been applied in multiple studies. In the SCS and proximity, it has been applied to investigate the impact of typhoons on the upper ocean temperature [Lin *et al.*, 2008], upwelling in the northern reaches of the Luzon Strait [Ko *et al.*, 2009], thermal structures in South China Sea [Chang *et al.*, 2010], and impact of eddies on the Kuroshio transport [Lee *et al.*, 2013].

Though tidal effect was much neglected in existing research on typhoon impacts, our preliminary numerical experiments pointed out the possible contribution from tides to enhance cold wakes. Therefore, the possible tidal impact is also considered. Eight tidal constituents (K1, O1, P1, Q1, K2, M2, N2, and S2) obtained from the Oregon State University Tidal Prediction Software [Egbert and Erofeeva, 2002] are applied.

The consequent internal tides, in addition to propagating away from the cold wake, also enhance cold wake intensity even after they have been filtered out through time averaging. The oscillating internal tides persistently enhance vertical mixing that brings up colder waters from below the mixed layer; the process transcends a tidal cycle. We see the necessity of including tides to enhance model realism (vertical mixing and mixed layer entrainment), not for the purpose of investigating intratidal variations. In displaying model results, tides are mostly filtered out by 48 h averaging to avoid sidetracking issues of tidal dynamics, which contained too many details to be included herein.

3. Atmospheric Forcing

The atmospheric forcing applied is the high-resolution Weather Research and Forecasting (WRF) model outputs, supplemented with Navy Operational Global Atmospheric Prediction System (NOGAPS) [Rosmond, 1992] products. The WRF model domain (Figure 1, inset) runs on a triple (54/18/6 km) nested grid system with finer interior grids moving with Megi to gain resolution. By applying the ensemble Kalman Filter (EnKF) method as used in Wu *et al.* [2010, 2012], the WRF model assimilated Megi's track from JTWC, SFMR (Stepped Frequency Microwave Radiometer), and dropsonde winds from both C-130 and Astra (DOTSTAR) [Wu *et al.*, 2005] aircrafts during the 2010 typhoon-tracking ITOP experiment. Though the ITOP aircraft observations were conducted only over the western North Pacific Ocean but not in the SCS, the large amount of aircraft observations significantly enhanced the high-resolution typhoon wind fields in WRF over the western North Pacific. Therefore, the subsequent wind field of Megi over the SCS was also much improved.

The 10 m wind and sea level air pressure from WRF domain are interpolated onto the ocean model grid and meshed with prediction from NOGAPS in areas outside the triple nested grid. The expected

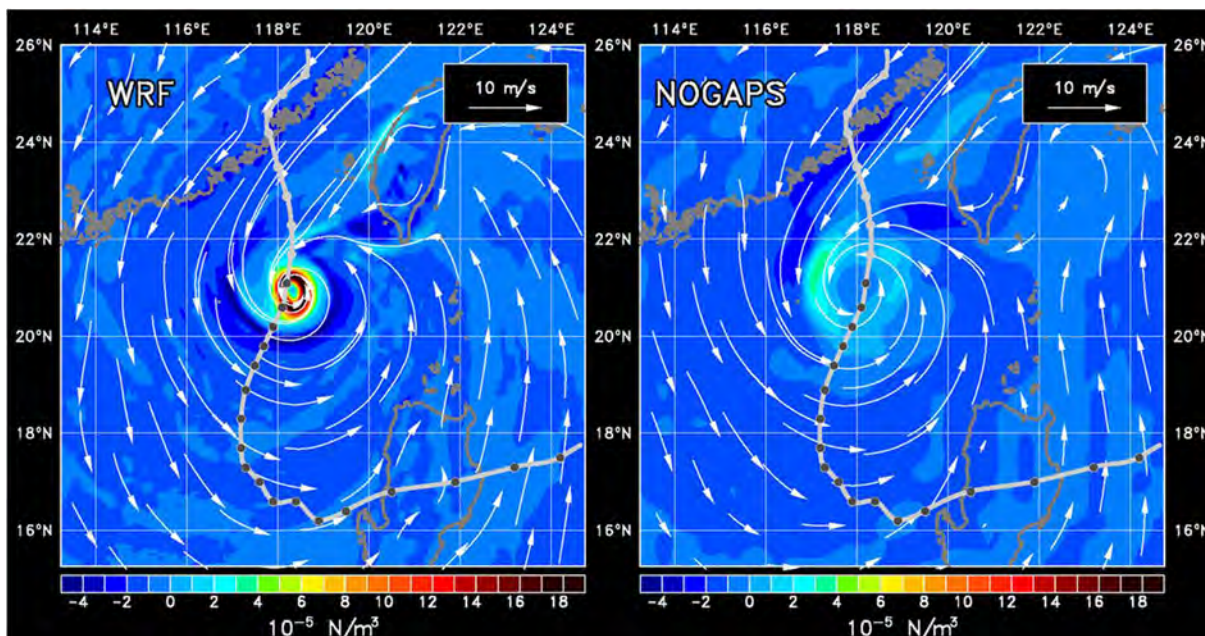


Figure 5. Wind stress curl in color and 10 m wind in vector at 0000 UTC 22 October 2010 produced by (left) WRF model and (right) NOGAPS. Megi's track is superimposed. The wind stress curl around Megi produced by the typhoon resolving WRF model is more than 5 times of that produced by 0.5° global NOGAPS.

underestimation of Megi's intensity by a global atmospheric prediction model such as NOGAPS is largely overcome. For example, at 0000 UTC 22 October the WRF model enhanced NOGAPS wind stress curl around Megi more than 5 times (Figure 5). Wind stress curl is tightly connected to Ekman pumping and cold wake development.

To cope with typhoon level wind stress in as simple a formula as possible, the wind stress vector ($\vec{\tau}$) is related to air density (ρ_a) and 10 m wind vector (\vec{u}) with a dimensionless drag coefficient (C_d) as $\vec{\tau} = \rho_a C_d |\vec{u}| \vec{u}$, where C_d follows the formulation of *Large et al.* [1994] but levels off abruptly once the wind speed exceeds 30 m/s as suggested by *Donelan et al.* [2004].

It is essential to improve Megi's intensity with the WRF model, without which the NOGAPS wind will be practically incapable of producing cold wakes that measure up to the observed strength. Figure 6 shows WRF daily 10 m wind and sea level pressure before, during, and after Megi's transit over the SCS. As illustrated, Megi weakened after passing Luzon but gradually regained its strength over the SCS, before weakening and losing its eyewall over the southern reaches of Taiwan Strait. Well before Megi approached Luzon, the winter NE monsoon ranging in excess of 10 m/s had already been developing over the northern reaches of the SCS. During the passing of Megi, Megi's wind field dominated. Few days after Megi's landfall and dissipation over southeast China, the dominance of the NE monsoon over the SCS resumed, with a high-pressure system moving south.

The simulation with improved atmospheric forcing, including 10 m wind stress and sea level air pressure, is conducted for the time period from 1 September 2010 to 1 November 2010. The period of Megi's transit during October 2010 is analyzed.

4. Upper Ocean Response in the SCS

Figure 7 shows snapshots of detided SST and surface currents from EASNFS before and after Megi entered the SCS, along with JTWC's best-track observations for Megi. Tides are filtered by 48 h averaging. On the western North Pacific Ocean side, the encroachment of meandering Kuroshio in the Luzon Strait and subsequent straight Kuroshio path along the east coast of Taiwan stood out. On the SCS side, before Megi's entrance to the SCS (Figure 7a), the northeast monsoon had already appeared over northern reaches,

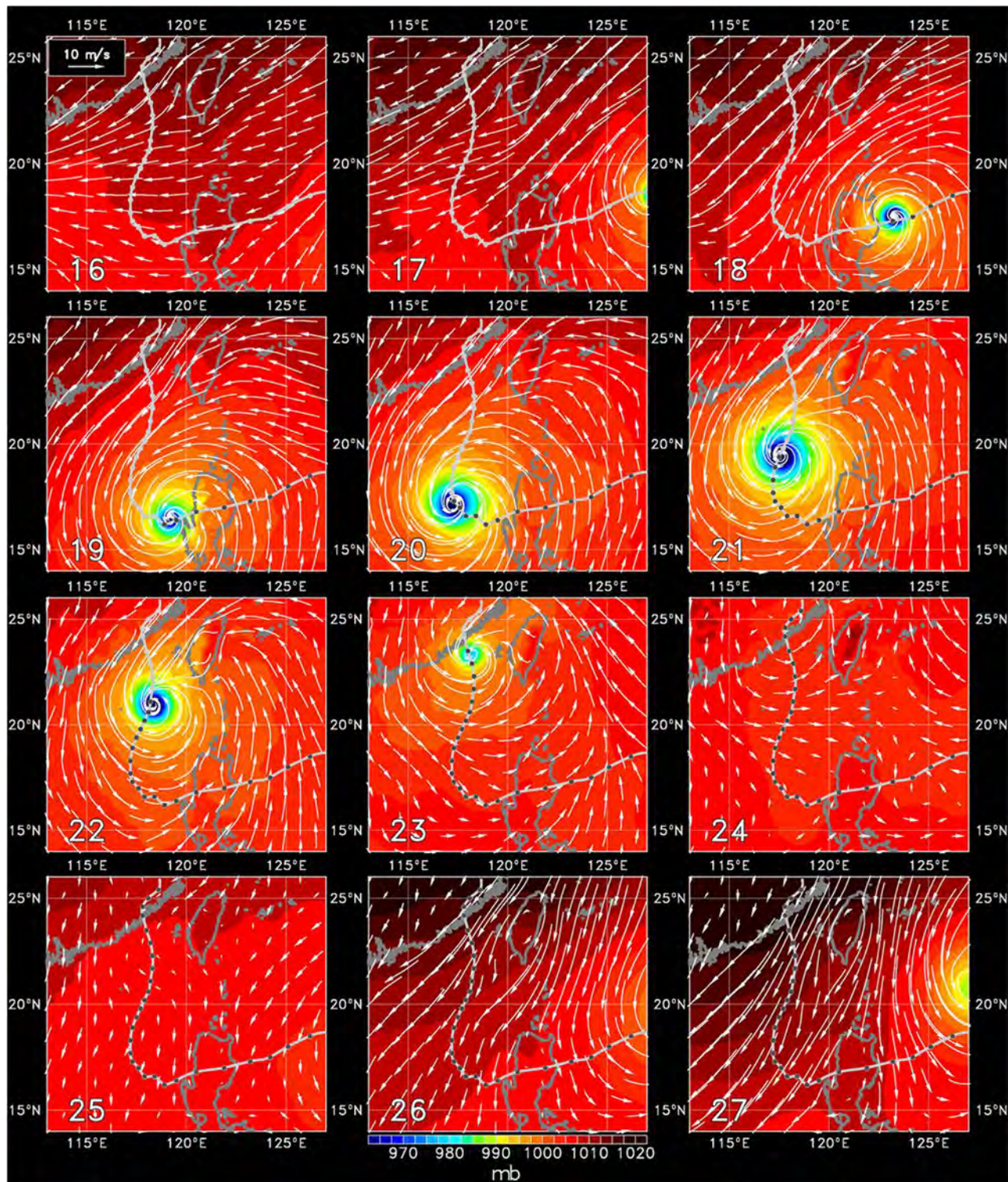


Figure 6. Daily snapshots of atmospheric forcing from WRF model (10 m wind vector and sea level air pressure in color) from 16 October 2010 00UTC (about 3 days before Megi’s entrance to SCS) to 27 October 2010 00UTC (about 4 days after Megi’s landfall on China). JTWC track is superimposed.

driving a southwestward (downwelling-favorable) coastal jet that brought increasingly colder water from north of the Taiwan Strait to spread along the southeast coast of China. After entering the SCS (Figures 7c and 7d), the northward moving Megi left a trail of intense north-south elongated cold wake behind.

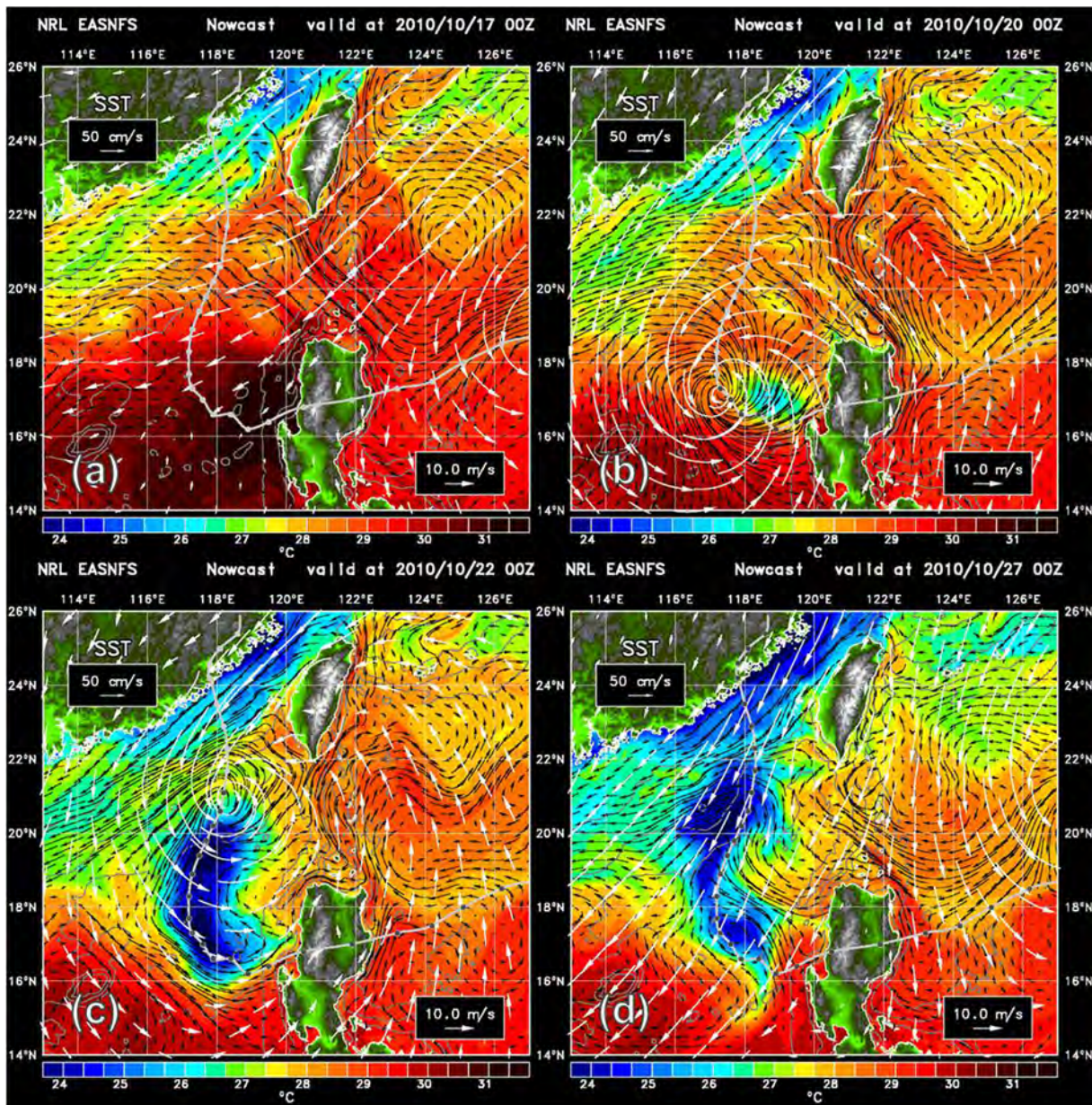


Figure 7. (a–d) Snapshots of 48 h averaged SST and surface current from EASNFS before and after Megi entered the SCS. Superimposed are wind vectors in white color from WRF model. Also shown is JTWC best-track for Megi with its center dotted every 6 h.

Circulation around the cold wake was mostly cyclonic. Shortly after Megi’s entrance (Figure 7b), the cold wake initially showed rightward bias relative to the track. As Megi turned northward, the cold wake began to spread more evenly across the track (Figure 7c). Well after Megi’s passage, there was a tendency for the cold wake to drift westward (i.e., to the left of the typhoon track), especially in the northern reaches of SCS (Figure 7d). The ambient surface current was southwestward in northern reaches, capable of moving the cold wake westward. Furthermore, northern reaches are over the steep continental slope, of which the topographic β effect (β_h^h) could conceivably move the cold wake anomaly westward or in the propagation direction of the topographic Rossby waves.

Borrowing the well-known propagation formula for nondispersive, barotropic planetary Rossby waves, we can use $C \approx -\beta_h / (k_x^2 + k_y^2)$ as a rough reference to scale the westward propagation speed of the cold wake, where horizontal wave numbers (k_x and k_y) can be estimated from the diameter ($D \sim 150$ km) of

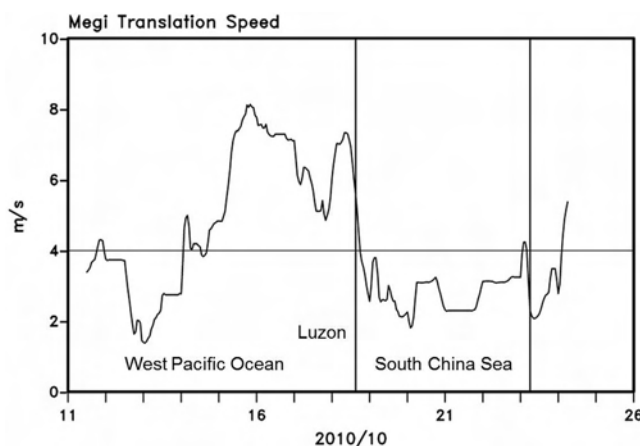


Figure 8. Translation speed of Megi estimated from JTWC best-track before and after it entered the SCS. Intercepts of two vertical lines mark the times Megi's center entered and left the SCS. Megi's translation speed in the SCS is well below 4 m/s, a condition suggested by Price [1981] as necessary for cross-track spread of a cold wake.

Megi's eye entered and left the SCS. Over the western North Pacific Ocean and Luzon, Megi's translation speed was well above 4 m/s. The cold wake was weak and rightward biased as observed by Lin *et al.* [2013]. Over the SCS, Megi's translation speed dropped quickly to below 4 m/s while curving from westward to northward. More symmetric across-the-track cold wake appearance occurred concurrently in satellite observation (Figure 3) and model prediction (Figure 7c) as suggested by Price [1981] and Zedler [2009].

Zooming into the three-dimensional cold wake structure when Megi had reached northern reaches of the SCS, Figure 9 shows 48 h averaged (a) temperature and currents at 150 m, (b) longitudinal-vertical section of temperature at 19.5°N, and (c) SSH and surface currents at 0000 UTC 22 October. At 150 m, the cyclonic circulation around the cold dome was much better defined but weaker (Figure 9a). Isotherm doming, ranging in excess of 100 m in height, extended well below 450 m in depth (Figure 9b). The doming was partly enhanced by internal tides, without which the magnitude of the subsurface doming height would be reduced (not shown). Concurrent SSH showed pronounced sea level depression associated with the cold wake (Figure 9c) implying a divergence of waters from its track.

5. Internal Kelvin Wave Around Luzon Island

The Megi-induced sea level depression must come from increased outflow or reduced inflow. Entering fall and winter, the Luzon Strait transport is characterized by a sizable inflow [e.g., Hsin *et al.*, 2012]. Our model suggested that Megi reduced inflow rather than enhanced outflow through the Luzon Strait, and the reduced inflow arose from an internal Kelvin wave propagation from west to east coast of Luzon Island.

Figure 10 shows daily snapshots of 48 h averaged vertical velocity and horizontal flow fields at 150 m after Megi entered the SCS, along with Megi's track and location. Upwelling (Ekman pumping) under the moving typhoon stood out as the most dominant signal. Cyclonic circulation around the cold dome area soon established after the moving Ekman pumping passed through the region. Trailing behind the strong Ekman pumping was weak downwelling along the track. In addition to the cold dome establishment, a patch of coastal downwelling soon appeared along the west coast of Luzon after Megi entered the SCS (Figure 10, top left). It then transmitted clockwise (in the right-bounded direction) to move out of the Luzon Strait. Subsurface downwelling should be accompanied by elevated sea level, and waters can be moved out of the Luzon Strait through the transmission. Estimating from the first baroclinic mode at the southern end of the Luzon Strait, the deformation radius is about 40 km and the phase speed is about 1.5 m/s. The clockwise transmission around northern Luzon (Figure 10) fits the estimates and therefore can be regarded as an internal Kelvin wave.

Zooming in, Figure 11 illustrates the three-dimensional features at 1200 UTC on 18 and 19 October. A zonal section along 17.8°N (off the west coast of Luzon) is marked in plan views at 150 m (Figure 11,

northern half of the cold wake, which is due to break up as an isolated eddy and moves westward during subsequent fission. The local β_h can be estimated from local Coriolis parameter (f) and north-south (y -) variation of water depth (h) as fh_y/h . The estimate leads to a C of about 30 cm/s or 26 km/d, which is comparable to the model-produced moving speed as we will see in Figure 13.

Figure 8 shows Megi's translation speed as a function of time derived from JTWC's best-track data. Intercepts by two vertical lines mark the times

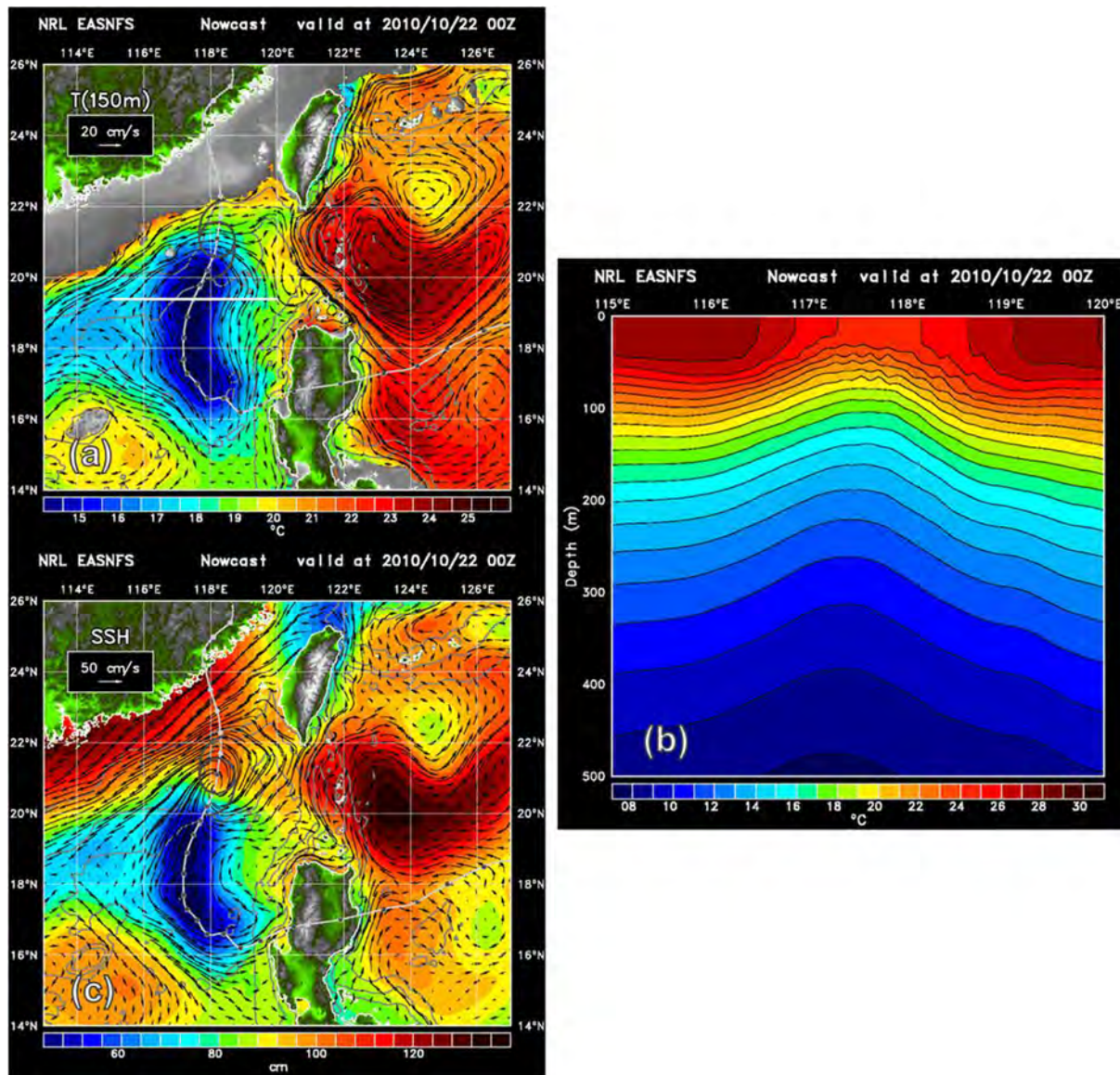


Figure 9. Detided (a) temperature and currents at 150 m, (b) longitudinal-vertical section of temperature at 19.5°N, and (c) SSH and surface currents at 0000 UTC 22 October 2010 from EASNFS. Longitudinal segment in Figure 9b is marked by a white line in Figure 9a. Superimposed on Figures 9a and 9c are Megi' track from JTWC and contemporaneous eye location (in hurricane symbol).

left). As the front half of Megi entered the SCS (Figure 11a), the wind (white arrows) was upwelling-favorable along the west coast of Luzon, driving southward coastal currents (black arrows), and upwelling (light red shading) as expected. Coastal isotherms were lifted in the top 130 m to support a southward coastal jet with a core speed in excess of 80 cm/s (Figure 11b). One day later, the rear half of Megi roamed over the coastal ocean off west Luzon (Figure 11, bottom). A patch of downwelling (in blue) began to show up at 150 m (Figure 11c). More information can be provided from vertical features in Figure 11d. Coastal isotherms showed remnants of upwelling in the top 50 m driven by the front half of Megi 1 day earlier, but much wider and deeper than 300 m downwelling below. Local downwelling-favorable wind in the rear half of Megi cannot drive such deep downwelling in about half a day. In other words, the downwelling must have arisen partially from remote influences or basin-wide constraints. This issue will be addressed later. The northward alongshore current in the top 75 m was not trapped by the coast; its core, ranging up to 1.4 m/s in speed, was more than 130 km offshore at this time and latitude (Figure 11d).

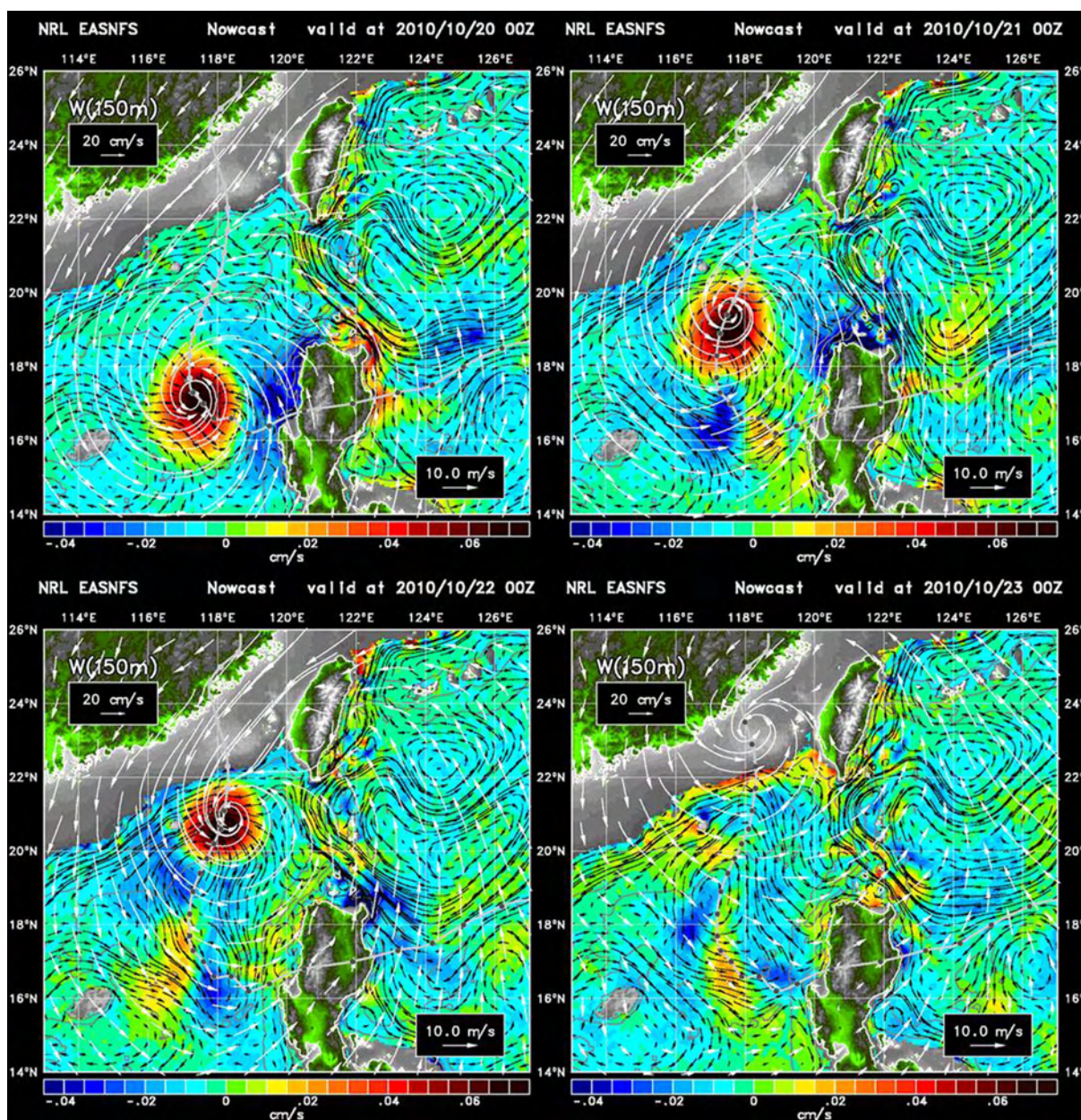


Figure 10. Daily snapshots from EASNFS of 48 h averaged vertical velocity in color and horizontal flow in vector (black) at 150 m during Megi’s transit in the SCS, along with Megi’s track from JTWC and WRF wind vectors (in white).

6. Luzon Strait Transport

Figure 12, also derived from the model, shows two types of depth-integrated Luzon Strait transport and area-averaged SSH as a function of time. All have been detided using 48 h running average. The transport covers either the entire Luzon Strait (in black curve) or within one baroclinic radius (40 km) north of the northern coast of Luzon (in blue curve). Area-averaged SSH is over the area surrounding Megi’s track from 114°E to 121°E and from 15°N to 23°N. Intercepts by two vertical lines mark the times when Megi entered and left the SCS. Well before Megi’s arrival, the strait-wide transport fluctuated about a westward inflow of 4 Sv, mainly due to the intrusion of Kuroshio. With the presence of winter northeast monsoon over northern reaches of the SCS (Figure 6), the strait-wide westward inflow increased further to about 7 Sv from 11 October to 17 October. Thereafter Megi’s arrival triggered first a slight volumetric increase followed by a

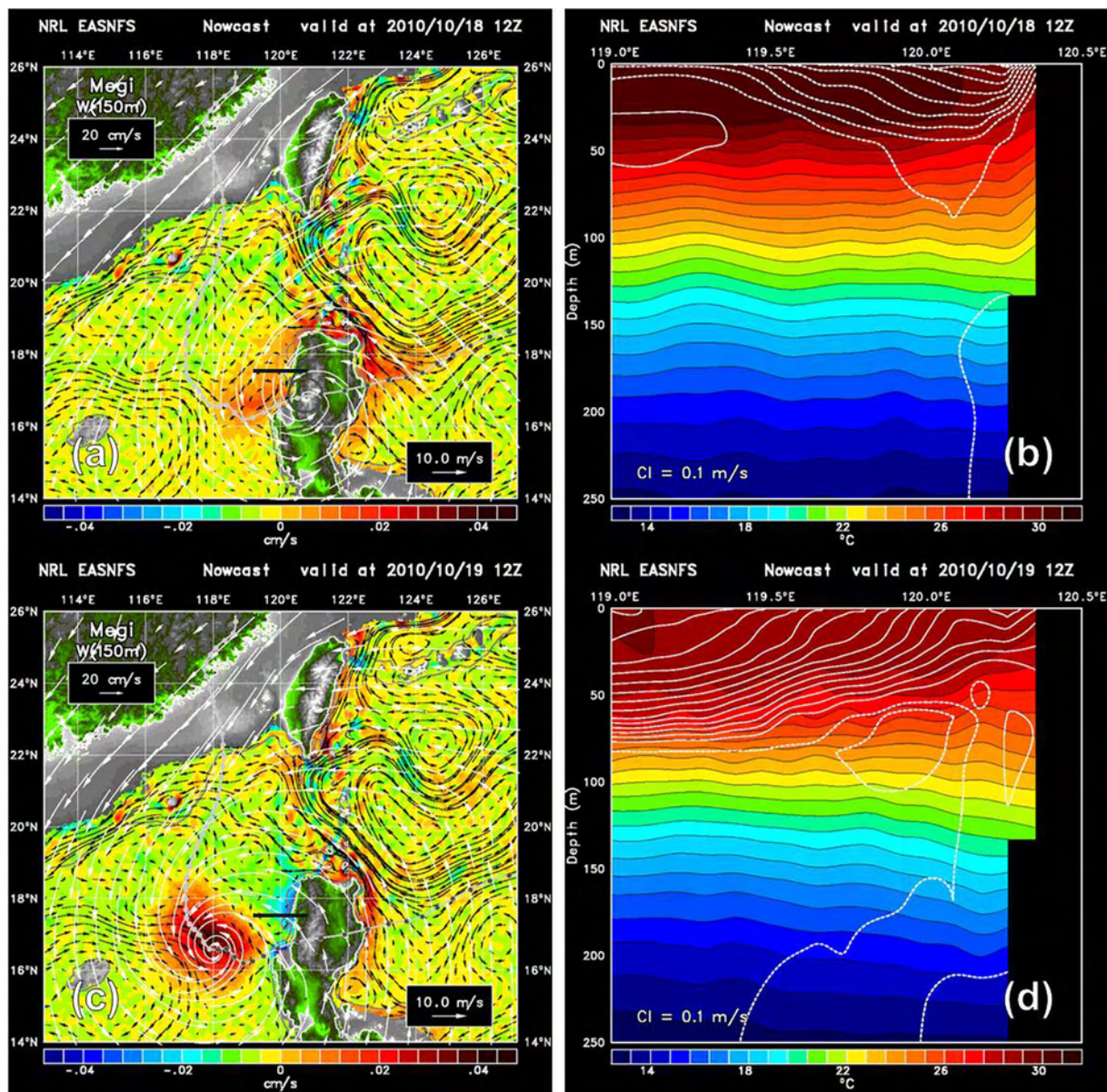


Figure 11. (a) Plan view of 10 m wind (white arrows) from WRF model, currents at 150 m (black arrows), vertical velocities at 150 m (in color) from EASNFS, and location of zonal-vertical section off west Luzon (thick black line) at 1200 UTC 18 October. (b) Corresponding zonal-vertical section of isotherms and meridional velocities along 17.5°N. (c, d) The same features at 1200 UTC 19 October. All oceanic variables are 48 h averaged. Northward (southward) currents are in solid (dashed) contours at intervals of 0.1 m/s.

sustained and sizable decrease of westward inflow. The initial slight increase of westward inflow was a downwind response driven by the northern half of Megi (Figure 11a). Subsequent profound decrease in westward inflow (on the order of 3.5 Sv) occurred when Megi was well over the SCS. After the westward inflow decreased to the minimum on 22 October, the rebound to the pre-Megi maximum (near 29 October) took about 7 days or 5 days after Megi exited SCS. The delay was profound.

In terms of sea level (red curve in Figure 12), the mostly pre-Megi and early-Megi increase in westward inflow continued to elevate SSH to a maximum on 20 October. Thereafter Megi-induced reduction in westward inflow drove a sustained SSH drop for about 7 days, 3 days after Megi exited the SCS.

In an open ocean environment, the sea level depression induced by a fast-moving typhoon will soon be refilled by return surface flow from nearly all directions. If the typhoon stagnates, the prolonged, localized

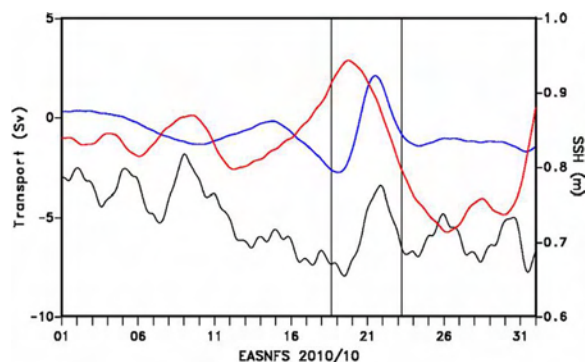


Figure 12. Depth-integrated, detided strait-wide Luzon Strait transport from EASNFS as a function of time (black curve), corresponding transport within one baroclinic radius of deformation (40 km) off northern Luzon (blue curve), and area-averaged detided EASNFS SSH in the northern South China Sea (114°E–121°E and 15°N–23°N, red curve). Intercepts by two vertical lines mark the times Megi’s center entered and left SCS. Negative transport indicates westward inflow. Megi expelled waters out of SCS and substantially reduced the inflow across the Luzon Strait. The depression of SSH followed. The expelled waters exited SCS mainly through a conduit within 40 km off northern coast of Luzon.

sea level depression may allow for a complete process of geostrophic adjustment before the storm moves away. After the adjustment the depression becomes a quasi-equilibrium state and the return flow would be delayed. In the case of a slow-moving typhoon over the SCS, the depression-induced water export through the Luzon Strait would soon disperse into the vast expanse of the western Pacific Ocean. As shown in Figure 12, red curve, refilling the void will likely be delayed substantially. If the theory stands, the delay is expected to allow for the geostrophic adjustment process

to establish a cyclonic eddy around the cold wake. When this happens, the rebound of inflow and sea level to the pre-typhoon level would be further delayed. Both our observations (Figure 4) and numerical results (Figure 9) support the foregoing arguments.

Megi-induced variation in westward inflow/eastward outflow was largely accounted for by variations within one baroclinic radius off northern Luzon. Within the radius the transport was typically negligible before or after Megi. A gush of westward inflow (from 15 October to 21 October) followed by another gush of eastward outflow (from 21 October to 24 October) within the deformation radius was adequate to account for the bottom-to-peak variation of strait-wide transport induced by Megi. The internal Kelvin wave is the conduit of choice and should be sufficiently nonlinear as linear ones do not transport water when depth-integrated.

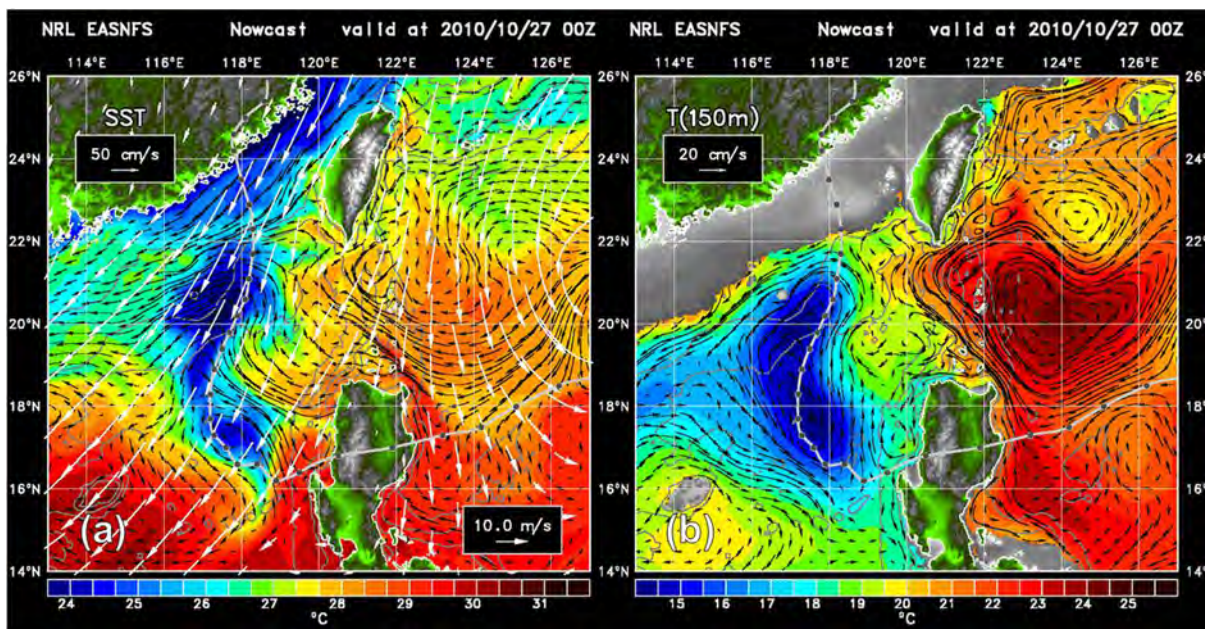


Figure 13. (a) Post-Megi surface winds (white vectors) from WRF model, 48 h averaged ocean currents (black vectors), and SST (colors) from EASNFS at 0000 UTC 27 October. Superimposed is the Megi’s track from JTWC dotted with 6 h eye locations. (b) Corresponding features without surface winds at 150 m. About 5 days after Megi’s passage, the cold wake (dome) has moved to the west of the track and fusion into two north-south oriented cyclonic eddies.

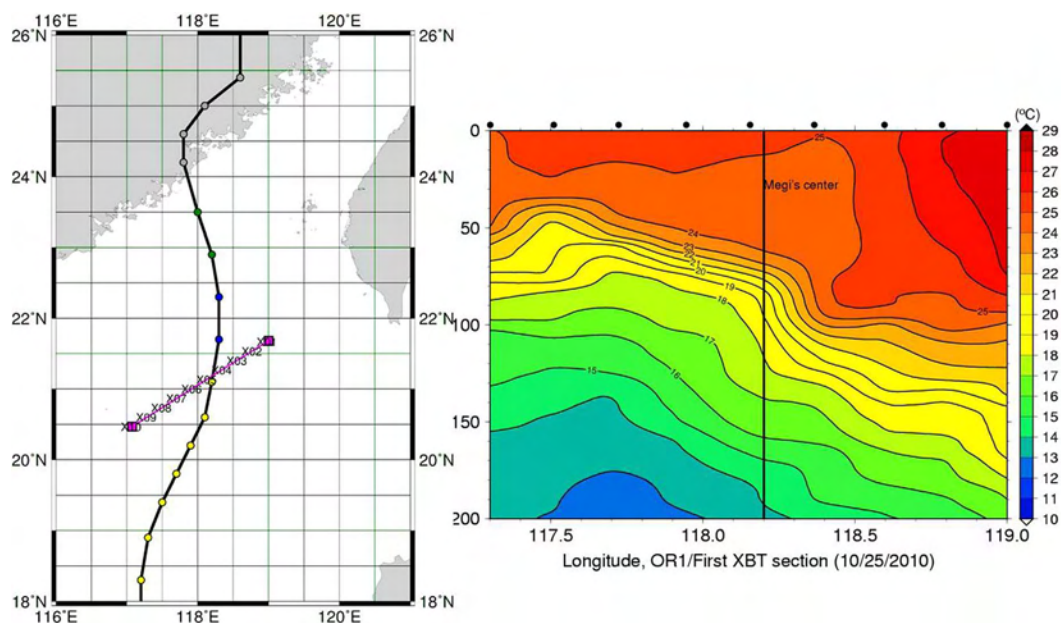


Figure 14. A cross-track XBT temperature transect from southwest to northeast on 25 October, 4.5 days after Megi passed the area. Vertical line on the left plot indicates Megi's track intercepted the transect. The cold dome was mostly on the left-hand side of the track, indicating a westward movement after the passage of Megi.

Megi's presence over the SCS caused a weeklong blockage of the developing northeast monsoon (Figure 6). The winter SCS throughflow from Luzon Strait to the Karimata Strait (between Borneo and Malaysia) was also disrupted (Figure 7). These factors may all have contributed to the Luzon Strait inflow decrease, which was several times more than adequate to account for the corresponding sea level drop in the northern SCS. The estimate can be sensitive to the time scale chosen, a topic requiring further studies. This is expected because, as Luzon Strait inflow decreases, water movement from northern to southern SCS can also be reduced to partially offset the sea level depression. Over time, the Luzon Strait inflow decrease must also be balanced by outflow decrease and/or inflow increase through other straits.

In terms of causality, Megi-induced responses were interwoven. On the atmospheric side, disturbances included (1) a low-pressure system that interrupted the developing northeast monsoon, and (2) the wind stress curl under Megi. In the SCS, major responses include (3) sizable inflow decrease through the Luzon Strait and (4) sea level drop, upwelling, and cyclonic circulation. Factors (1) and (2) came in one package and seemed difficult to separate. Both (1) and (2) could induce (3). It is well known that (2) can produce (4). Between (3) and (4), which one was the primary driving force? The causality issue is difficult to sort out. In this light, our perspective is inevitably a little subjective. We did not attempt to separate the effects of (1) and (2) on the SCS. Although (2) could lead to (4) and (1) could lead to (3) independently, we further suggested a feedback mechanism that (3) enhanced and sustained (4), simply because the effect of (3) is several times larger than what is needed to produce (4) and sea level depression in (4) eventually rebounded in time.

7. Cold Dome Fission

Megi left a trail of north-south elongated cold wake, of which the major semiaxis (of about 220 km) far exceeded the characteristic baroclinic Rossby radius (of about 60 km) for central SCS [Cai *et al.*, 2008]. Fission may follow. Figure 13 shows post-Megi surface winds, 48 h averaged ocean currents, and SST at 0000 UTC 27 October in Figure 13a and corresponding features without surface winds at 150 m in Figure 13b. At this time the northeast monsoon had resumed, and the surface coastal current off southeast China was southwestward in response to the northeast monsoon (Figure 13a). The tendency for the northern portion of the cold wake to drift westward is evident, most likely because the ambient current is westward and the topographic β dispersion of the continental slope is mostly westward.

Seagoing measurements lent support. Figure 14 was derived from an XBT temperature transect (from southwest to northeast) taken by the Taiwanese research vessel OR1 during 25 October, about 4.5 days after Megi passed the area. The view was northwestward. The transect cut through Megi's track from southwest to northeast. The longitude spread was shown in the horizontal axis of Figure 14. The anticipated cold water doming was mostly on the left-hand side of Megi's track, indicating its westward movement after Megi moved northward. The westward drift, however, is expected to be partially blocked by the shoaling bottom to the west.

The cold wake fission split the elongated cold dome into two north-south aligned cyclonic eddies at the surface. At 150 m depth (Figure 13b), the fission and the westward drift of consequent northern eddy were less distinct as the ambient southwestward coastal current weakened at this depth. From the theoretical point of view, the cyclonic circulation in and around the Megi-induced cold dome was not energetic enough to drive a strong fission.

In an open ocean environment, an oversized patch of density anomaly often sets off a cascade of fissions, if it is energetic enough (the density contrast relative to surroundings is high); the end scale of choice is the baroclinic Rossby radius of deformation [e.g., *Chao and Shaw*, 1999]. If the ambient ocean is relatively quiescent, two cold (cyclonic) eddies would corotate about each other in a counterclockwise fashion [e.g., *Griffiths and Hopfinger*, 1986]. In the present setting, the ambient current, the shoaling bottom nearby, and the topographic β dispersion of the underlying continental slope all present complications to, and deviations from, the idealized scenario.

8. Conclusions

Typhoon Megi (2010) entered the SCS from west coast of Luzon on 18 October, turned from westward to northward and made the second landfall over southeast China on 23 October. Moving from the western North Pacific Ocean to the SCS resulted in weaker intensity with slower typhoon translation speed prior to its northward recurvature. The cold wake began to appear on both sides of the track and grow spontaneously in strength. It then propagated to the left of the typhoon track, an interesting phenomena contrary to the well-known rightward bias of typhoon-induced cold wake over the northern hemisphere [*Price*, 1981; *Lin et al.*, 2003b]. Examining the cause, the slow translation speed in the SCS is expected to induce cross-track distribution of the cold wake [*Price*, 1981; *Zedler*, 2009]. Further, the cold wake owed its intensity to the preconditioned shallow thermocline and waters expelled by Megi from the SCS. The latter manifested a gush of internal Kelvin wave moving clockwise around northern Luzon to export waters through the Luzon Strait. The consequent sea level depression in the SCS lasted and presented a favorable condition for the development of cyclonic eddy or cold dome. Fission of the north-south elongated cold dome resulted afterward and produced two cold eddies that dissipated slowly thereafter.

The documented sequence of events after Megi (2010) may not be generalized to other typhoons at the present time, noting that each typhoon is unique in its path, size, translation speed, and intensity. Nevertheless, this research presents the interesting interplay between NE monsoon, late-season typhoon Megi, and the unique topographical effect in the SCS. Limited supporting evidences from the past are also encouraging. For example, Typhoon Fengshen (2008) followed a similar track over the SCS in 2008. The consequent post-typhoon sea level depression enhanced the Kuroshio water meandering into the SCS and suggested to have induced an anomalous upwelling event in the southernmost bay of Taiwan [*Ko et al.*, 2009]. The phenomenal cold wake growth trailing behind Typhoon Kai-Tak (2000) could have been preconditioned by a shallow SCS thermocline, along with very slow translation speed despite its weak intensity [*Lin et al.*, 2003a; *Chiang et al.*, 2011]. With improved typhoon resolution in this numerical investigation, the internal Kelvin wave export of waters through the Luzon Strait came to light. Is this mode of typhoon-induced export canonical? Are favorable growth and retention of cold wakes in the SCS equally active for other typhoons coming from more southern or northern routes? Our efforts along this line of investigation are ongoing.

References

- Cai, S., X. Long, R. Wu, and S. Wang (2008), Geographical and monthly variability of the first baroclinic Rossby radius of deformation in the South China Sea, *J. Mar. Syst.*, *74*, 711–720, doi:10.1016/j.jmarsys.2007.12.008.

Acknowledgments

D.S.K. and S.-Y.C. were supported by the U.S. Office of Naval Research (ONR) grants N00014-08WX-2-1170 and N00014-09-1-0623, respectively.

C.-C.W. was supported by Taiwan's National Science Council (NSC) grant NSC97-2111-M-002-397 016-MY3 and ONR grant N00014-10-1-0725. I-I Lin was supported by NSC grants NSC101-2111-M-002/-001-MY2 and NSC101-2628-M-002/-001-MY4; 102R7803 and ORN travel grant. Thanks to lam-Fei Pun for the ORI XBT data. We also like to acknowledge the late David T. Y. Tang who was the leader of the ITOP Taiwan term and led the OR1 cruise to the SCS. Helpful comments from Jim Price and anonymous reviewers are appreciated.

- Carnes, M. R., D. N. Fox, R. C. Rhodes, and O. M. Smedstad (1996), Data assimilation in a North Pacific Ocean monitoring and prediction system, in *Modern Approaches to Data Assimilation in Ocean Modeling*, Elsevier Oceanogr. Ser., edited by P. Malanotte-Rizzoli, pp. 319–345, Elsevier, Amsterdam, doi:10.1016/S0422-9894(96)80015-8.
- Chang, Y.-T., T. Y. Tang, S.-Y. Chao, M.-H. Chang, D. S. Ko, Y. J. Yang, W.-D. Liang, and M. J. McPhaden (2010), Mooring observations and numerical modeling of thermal structures in the South China Sea, *J. Geophys. Res.*, *115*, C10022, doi:10.1029/2010JC006293.
- Chao, S.-Y., and P.-T. Shaw (1999), Fission of heton-like vortices under sea ice, *J. Oceanogr.*, *55*, 65–78.
- Chen, X., D. Pan, X. He, Y. Bai, and D. Wang (2012), Upper ocean responses to category 5 typhoon Megi in the western north Pacific, *Acta Oceanol. Sin.*, *31*(1), 51–58.
- Chiang, T.-L., C.-R. Wu, and L.-Y. Oey (2011), Typhoon Kai-Tak: An ocean's perfect storm, *J. Phys. Oceanogr.*, *42*, 221–233, doi:10.1175/2010JPO4518.1.
- Chu, P. C., J. M. Veneziano, C. Fan, M. J. Carron, and W. T. Liu (2000), Response of the South China Sea to Tropical Cyclone Ernie 1996, *J. Geophys. Res.*, *105*, 13,991–14,009.
- D'Asaro, E. A., et al. (2011), Typhoon-ocean interaction in the Western North Pacific, Part 1, *Oceanography*, *24*, 24–31, doi:10.5670/oceanog.2011.91.
- D'Asaro, E. A., et al. (2013), Impact of typhoons on the ocean in the Pacific: ITOP, *Bull. Am. Meteorol. Soc.*, doi:10.1175/BAMS-D-12-00104.1, in press.
- Donelan, M. A., B. K. Haus, N. Reul, W. J. Plant, M. Stiassne, H. C. Graber, O. B. Brown, and E. S. Saltzman (2004), On the limiting aerodynamic roughness of the ocean in very strong winds, *Geophys. Res. Lett.*, *31*, L18306, doi:10.1029/2004GL019460.
- Egbert, G. D., and S. Y. Erofeeva (2002), Efficient inverse modeling of barotropic ocean tides, *J. Atmos. Oceanic Technol.*, *19*, 183–204, doi:10.1175/1520-0426(2002)019<0183:EIMOBO>2.0.CO;2.
- Fox, D. N., W. J. Teague, C. N. Barron, M. R. Carnes, and C. M. Lee (2002), The Modular Ocean Data Assimilation System (MODAS), *J. Atmos. Oceanic Technol.*, *19*, 240–252, doi:10.1175/1520-0426(2002)019<0240:TMODAS>2.0.CO;2.
- Griffiths, R. W., and E. J. Hopfinger (1986), Experiments with baroclinic vortex pairs in a rotating fluid, *J. Fluid Mech.*, *173*, 501–518.
- Hsin, Y.-C., C.-R. Wu, and S.-Y. Chao (2012), An updated examination of the Luzon Strait transport, *J. Geophys. Res.*, *117*, C03022, doi:10.1029/2011JC007714.
- Ko, D. S., P. J. Martin, C. D. Rowley, and R. H. Preller (2008), A real-time coastal ocean prediction experiment for MREA04, *J. Mar. Syst.*, *69*, 17–28, doi:10.1016/j.jmarsys.2007.02.022.
- Ko, D. S., S.-Y. Chao, P. Huang, and S. F. Lin (2009), Anomalous upwelling in Nan Wan: July 2008, *Terr. Atmos. Oceanic Sci.*, *20*, 839–852, doi:10.3319/TAO.2008.11.25.01(Oc).
- Large, W. G., J. C. McWilliams, and S. C. Doney (1994), Oceanic vertical mixing: A review and a model with a nonlocal boundary layer parameterization, *Rev. Geophys.*, *32*, 363–403.
- Lee, I.-H., D. S. Ko, Y.-H. Wang, L. Centurioni, and D.-P. Wang (2013), The mesoscale eddies and Kuroshio transport in the western North Pacific east of Taiwan from 8-year (2003–2010) model reanalysis, *Ocean Dyn.*, *63*, 1027–1040, doi:10.1007/s10236-013-0643-z.
- Lin, I.-I., W. T. Liu, C. C. Wu, G. T. F. Wong, C. Hu, Z. Chen, W. D. Liang, Y. Yang, and K. K. Liu (2003a), New evidence for enhanced ocean primary production triggered by tropical cyclone, *Geophys. Res. Lett.*, *30*(13), 1718, doi:10.1029/2003GL017141.
- Lin, I.-I., W. T. Liu, C. C. Wu, J. C. H. Chiang, and C. H. Sui (2003b), Satellite observations of modulation of surface winds by typhoon-induced upper ocean cooling, *Geophys. Res. Lett.*, *30*(3), 1131, doi:10.1029/2002GL015674.
- Lin, I.-I., C.-C. Wu, I.-F. Pun, and D. S. Ko (2008), Upper ocean thermal structure and the western North Pacific category-5 typhoons, part I: Ocean features and category-5 typhoon's intensification, *Mon. Weather Rev.*, *136*, 3288–3306, doi:10.1175/2008MWR2277.1.
- Lin, I.-I., P. Black, J. F. Price, C.-Y. Yang, S. S. Chen, C.-C. Lien, P. Harr, N.-H. Chi, C.-C. Wu, and E. A. D'Asaro (2013), An ocean coupling potential intensity index for tropical cyclones, *Geophys. Res. Lett.*, *40*, 1878–1882, doi:10.1002/grl.50091.
- Martin, P. J. (2000), A description of the navy coastal ocean model version 1.0, *NRL Rep. NRL/FR/7322-00-9962*, 42 pp., Nav. Res. Lab., Stennis Space Cent., Miss.
- Price, J. F. (1981), Upper ocean response to a hurricane, *J. Phys. Oceanogr.*, *11*, 153–175.
- Pun, I. F., Y.-T. Chang, I.-I. Lin, T.-Y. Tang, and R.-C. Lien (2011), Typhoon-ocean interaction in the Western North Pacific, Part 2, *Oceanography*, *24*, 32–41, doi:10.5670/oceanog.2011.92.
- Rosmond, T. E. (1992), The design and testing of the Navy Operational Global Atmospheric Prediction System, *Weather Forecast*, *7*, 262–272, doi:10.1175/1520-0434(1992).
- Shang, S. L., L. Li, F. Sun, J. Wu, C. Hu, D. Chen, X. Ning, Y. Qiu, C. Zhang, and S. Shang (2008), Changes of temperature and bio-optical properties in the South China Sea in response to typhoon Lingling, 2001, *Geophys. Res. Lett.*, *35*, L10602, doi:10.1029/2008GL033502.
- Tseng, Y. H., S. Jan, D. E. Dietrich, I. I. Lin, Y.-T. Chang, and T. Y. Tang (2010), Modeled oceanic response and sea surface cooling to typhoon Kai-Tak, *Terr. Atmos. Oceanic Sci.*, *21*, 85–98, doi:10.3319/TAO.2009.06.08.02(IWNOP).
- Wentz, F. J., C. Gentemann, D. Smith, and D. Chelton (2000), Satellite measurements of sea surface temperature through clouds, *Science*, *288*, 847–850.
- Wu, C.-C., et al. (2005), Dropwindsonde observations for typhoon surveillance near the Taiwan region (DOTSTAR): An overview, *Bull. Am. Meteorol. Soc.*, *86*, 787–790.
- Wu, C.-C., G.-Y. Lien, J.-H. Chen, and F. Zhang (2010), Assimilation of tropical cyclone track and structure based on the Ensemble Kalman Filter (EnKF), *J. Atmos. Sci.*, *67*, 3806–3822, doi:10.1175/2010JAS3444.1.
- Wu, C.-C., Y.-H. Huang, and G.-Y. Lien (2012), Concentric eyewall formation in Typhoon Sinlaku (2008). Part I: Assimilation of T-PARC data based on the ensemble Kalman filter (EnKF), *Mon. Weather Rev.*, *140*, 506–527, doi:10.1175/MWR-D-11-00057.1.
- Zedler, S. E. (2009), Simulations of the ocean response to a Hurricane: Nonlinear processes, *J. Phys. Oceanogr.*, *39*, 2618–2634.
- Zheng, G., and D. Tang (2007), Offshore and nearshore chlorophyll increases induced by typhoon winds and subsequent terrestrial rain-water runoff, *Mar. Ecol. Prog. Ser.*, *333*, 61–74, doi:10.3354/meps333061.